Research Article Vol. 13, No. 10 / 1 Oct 2023 / Optical Materials Express 2798
Optical Materials EXPRESS

Trapping-induced quantum beats in a van-der-Waals heterostructure microcavity observed by two-dimensional micro-spectroscopy

DONGHAI LI,[1,2,13] HANGYONG SHAN,[3] HEIKO KNOPF,[4,5,6] KENJI WATANABE,[7] TAKASHI TANIGUCHI,[8] YING QIN,[9] SEFAATTIN TONGAY,[9] FALK EILENBERGER,[4,5,6] SVEN HÖFLING,[10,11] CHRISTIAN SCHNEIDER,[3,10,14] AND TOBIAS BRIXNER[2,11,12,15]

[1]*University of Science and Technology of China, Hefei National Research Center for Physical Sciences at the Microscale, 230026 Hefei, China*
[2]*Universität Würzburg, Institut für Physikalische und Theoretische Chemie, Am Hubland, 97074 Würzburg, Germany*
[3]*University of Oldenburg, Institute of Physics, 26129 Oldenburg, Germany*
[4]*Friedrich Schiller University, Institute of Applied Physics, Abbe Center of Photonics, Albert-Einstein-Straße 15, 07745 Jena, Germany*
[5]*Fraunhofer-Institute for Applied Optics and Precision Engineering IOF, Albert-Einstein-Straße 7, 07745 Jena, Germany*
[6]*Max Planck School of Photonics, Albert-Einstein-Straße 7, 07745 Jena, Germany*
[7]*National Institute for Materials Science, Research Center for Electronic and Optical Materials, 1-1 Namiki, Tsukuba, Ibaraki 305-0044, Japan*
[8]*National Institute for Materials Science, Research Center for Materials Nanoarchitectonics, 1-1 Namiki, Tsukuba, Ibaraki 305-0044, Japan*
[9]*Arizona State University, Materials Science and Engineering, School of Engineering of Matter, Transport, and Energy, Tempe, AZ 85287, USA*
[10]*Universität Würzburg, Technische Physik, Am Hubland, 97074 Würzburg, Germany*
[11]*Universität Würzburg, Wilhelm Conrad Röntgen Research Center for Complex Material Systems, Am Hubland, 97074 Würzburg, Germany*
[12]*Universität Würzburg, Center for Nanosystems Chemistry (CNC), Theodor-Boveri-Weg, 97074 Würzburg, Germany*
[13]*lidonghai@ustc.edu.cn*
[14]*christian.schneider@uol.de*
[15]*brixner@uni-wuerzburg.de*

Abstract: Spatial confinement has been frequently engineered to control the flow and relaxation dynamics of exciton polaritons. While widely investigated in GaAs microcavities, exciton-polariton coupling between discretized polariton modes arising from spatially confined 2D crystals been has been less exhaustively studied. Here, we use coherent 2D photoluminescence-detected micro-spectroscopy to detect oscillating 2D peaks exclusively from a spatial trap in a microcavity with an embedded van-der-Waals heterostructure at room temperature. We observe a wide variation of oscillatory phases as a function of spectral position within the 2D spectrum, which suggests the existence of a coupling between the discretized polariton modes. The latter is accompanied by the generation of coherent phonons.

1. Introduction

Exciton polaritons are bosonic quasiparticles resulting from strong coupling between excitons and photons in a microcavity [1]. Because of the relatively low effective mass inherited from

#492545 https://doi.org/10.1364/OME.492545
Journal © 2023 Received 6 Apr 2023; revised 23 Jul 2023; accepted 10 Aug 2023; published 14 Sep 2023

Optical Materials EXPRESS

the cavity photons, which is approximately five orders of magnitude smaller than that of a free electron, exciton polaritons can condensate at elevated temperatures even when they are out of equilibrium with the environment [2,3]. Another consequence of the low mass of polaritons is their ultrafast photon-like velocity, which makes it easy for exciton polaritons to escape from the excitation area, hence reducing the scattering rates. In order to control and direct the flow of exciton polaritons, spatial confinements have been introduced by a variety of techniques [4–7]. It was suggested that the polariton relaxation mechanism can be enhanced in the presence of spatial confinement, promoting the thermalization and the condensation processes [8,9]. In addition, confinement is often accompanied by the appearance of polariton band discretization, which substantially changes the dynamical mechanism of energy transfer between discretized polariton modes as well as their interactions with phonons [10].

In GaAs microcavities, polariton trapping and engineering has been established and is widely investigated [11]. The role played by phonons on the dynamical control of the trapped polaritons in the confined microcavity systems has attracted extensive attention [5,12–17]. Population transfer between discretized polariton modes can be enhanced via an incoherent interaction with an acoustic phonon bath [12,13] or via a coherent interaction with longitudinal optical phonons [15]. Coherent interaction between microcavity polaritons and acoustic phonons can even form tunable polariton superlattices to confine the polaritons and modulates their dynamics [5,14]. Recent work demonstrated that a interaction between a longitudinal phonon mode and spatially confined polariton modes can not only modulate the polariton dynamics but also give rise to efficient polariton-to-phonon conversion, paving the way for new hybrid designs for polariton-driven phonon lasers [18].

Recently, transition metal dichalcogenide (TMD) monolayers and their van-der-Waals heterostructures have emerged as ideal materials for room temperature polaritonics [19–21], owing to their highly interesting excitonic properties, e.g., enormous binding energies and giant oscillator strength. Utilizing spatial confinement to influence the polariton condensation in TMD microcavities at room temperature has been reported in a monolayer WSe_2 microcavity [22], where a clear onset of spatial coherence has been observed in a trap. However, the investigation of microscopic coupling mechanisms between discretized polariton modes and phonons in TMD microcavities has not been reported to the best of our knowledge.

Coherent two-dimensional (2D) electronic spectroscopy is a powerful tool for investigating vibrational/vibronic coupling and many-body interactions via quantum beating signals [23–27]. Examples are photosynthetic complexes [28–31], artificial light-harvesting systems [32,33], single-walled carbon nanotubes [34], or atomically thin semiconductors [35,36]. When studying quantum beats, the time-domain signal can provide additional information via the oscillation period, dephasing time, and phase. In particular, phase information is not available in linear frequency-domain signals. Therefore, it is of interest to identify, in time domain, the coherences after excitation of discretized polariton modes in 2D semiconductor microcavities. The challenges for such an observation are how to achieve sufficiently high temporal and spatial resolution at the same time.

In this work, we study a WSe_2 van-der-Waals heterostructure embedded in a microcavity. The sample exhibits clear spectroscopic signatures of polariton trapping at room temperature. Using coherent 2D micro-spectroscopy, we obtain time-dependent spectra with a submicron spatial resolution as well as 20-fs temporal resolution and observe oscillating behavior of diagonal peaks. Importantly, wide phase variations of peak oscillations were observed. These suggest a coupling between the trapped polariton modes mediated by the coherent interaction with an inter-layer phonon mode.

Optical Materials EXPRESS

2. Experimental methods

Coherent 2D micro-spectroscopy adds submicron spatial resolution to coherent 2D spectroscopy by carrying out the experiment in an optical microscope [37–39]. It is worth noting that, compared to coherently detected 2D spectroscopy that relies on the detection of emission from the third-order polarization of the sample, 2D micro-spectroscopy employs a collinear four-pulse geometry and detects the intensity of an incoherent photoluminescence (PL) signal. Then, 2D Fourier transformation of the PL signal with respect to the inter-pulse "coherence" time delays between the first and second pulse as well as between the third and fourth pulse can be used to recover 2D spectra as a function of the "population" time delay between the second and the third pulse.

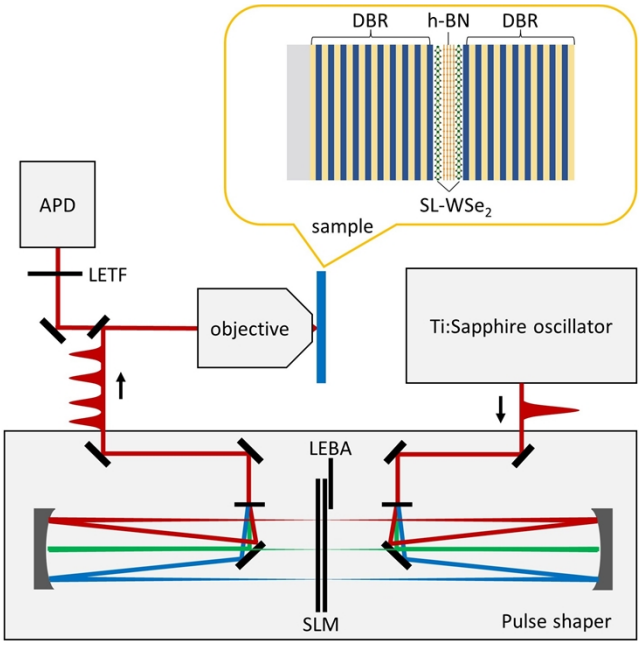

Fig. 1. Schematic illustration of the experimental setup. The orange inset at the top shows the structure of the studied microcavity with an embedded WSe_2 van-der-Waals heterostructure. Abbreviations: avalanche photodiode (APD), low-energy-blocking aperture (LEBA), low-energy-transmission filter (LETF), spatial light modulator (SLM) based on a one-dimensional double-layer liquid-crystal display (LCD), distributed Bragg reflector (DBR), single-layer WSe_2 (SL-WSe_2), hexagonal boron nitride (h-BN).

A schematic illustration of the experiment is shown in Fig. 1. Briefly, an ultrashort laser pulse, generated by a Ti:sapphire oscillator, was split into four collinear pulses by a liquid-crystal-display-(LCD-)based pulse shaper and coupled into a microscope objective with a numerical aperture of NA = 1.4. The PL emerging from the sample was collected by the same objective. Note that the reflected laser beam from the sample surface also entered the objective along with the PL signal. In order to completely filter out the reflected laser beam before it was incident on the avalanche photodiode (APD), we first used a low-energy-blocking aperture (LEBA in Fig. 1) in the Fourier plane of the pulse shaper to block out excitation light below 1.615 eV, while a low-energy-transmission filter (LETF) with a cut-off energy of 1.604 eV was placed in front of the APD to filter out the reflected excitation light from the sample. A detailed description of the setup can be found in previous work [37]. Apart from spatially resolved 2D spectra, the setup

Optical Materials EXPRESS

was also adapted to acquire spatial maps of the PL intensity from the sample simply by turning off the pulse shaper and scanning the lateral sample position.

3. Results and discussion

The studied sample was a microcavity with an embedded WSe_2 van-der-Waals heterostructure. The WSe_2/h-BN/WSe_2 heterostructure was composed of two WSe_2 monolayers separated by ~5-nm-thick h-BN and sandwiched between two distributed Bragg reflectors, as shown schematically in Fig. 1 (inset). More details of the sample preparation can be found in previous work [22,40].

Figure 2(a) shows a spatial map of the PL intensity of the sample, which was measured using the 2D micro-spectroscopy setup with the pulse shaper turned off. The inhomogeneity of the PL intensity distribution can be explained by inherent spatial confinements originally existing on the sample, which resulted in trapping of polaritons at particular positions and, thus, the inhomogeneity of relaxation efficiency and PL intensity. We then conducted a further optical modification of the sample by irradiating it with intense laser pulses (with a peak excitation intensity of ~500 GW/cm^2). During the optical modification, we monitored the PL microscopy image of the sample in real time. The optical modification was short in time, much shorter than the time to totally destroy the sample, but enough to lead to a change in optical behavior. After the modification process, the polariton trapping effect was dramatically enhanced: Only two hot spots could be observed across the sample area as shown in Fig. 2(b) (with the sample outline indicated by the white dashed lines), indicating that deeper traps were formed by the irradiation of high-power pulses at these two positions. This phenomenon can be explained by the thermal effect: Photoexcitation causes localized heating, leading to further deepening of the existing cracks and the formation of distinct potential energy traps in certain areas. The size of the hot spots (~1 μm) equals to the spatial resolution of the PL-imaging microscopy, thus defines the upper bound for the lateral extension of the polariton traps.

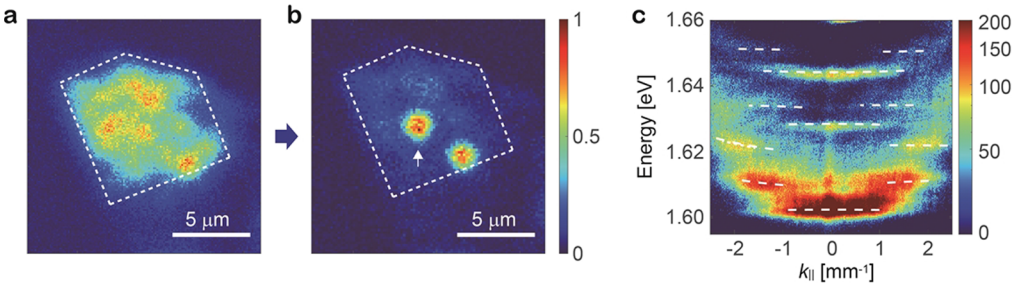

Fig. 2. Linear PL characterization of the sample. a,b, Spatial map of the PL intensity of the sample before (a) and after (b) the optical modification with intense laser pulses, with the white dashed pentagon indicating the area of the sample. The white arrow indicates the spot used in 2D spectroscopy. c, Energy-momentum-resolved map of the PL intensity. The white dashed lines are the fitting results of the maxima of the polariton dispersion curves, indicating the discretization of polariton dispersion.

To further characterize the sample, an energy-momentum-resolved map of the PL intensity (Fig. 2(c)) was measured by conducting a standard back-Fourier-plane imaging experiment. In the setup, a first lens (NA = 0.6) on top of the sample maps the momentum-dependent information at its back-focal plane, and a second and a third lens project this information into the focal plane (slit) of a spectrometer. In the energy-momentum-resolved PL map, three polariton branches can be identified via their main peaks for $k_{||} = 0$, located at ~1.605 eV, ~1.630 eV, and ~1.643 eV. We have demonstrated in previous work that the multiple polariton branches result from a three-fold hybridization between excitons, cavity photon, and optical phonons [41,42]. In addition, we find

Optical Materials EXPRESS

step-like dispersion (indicated by the dashed white curves in Fig. 2(c)) on each of the polariton branches at $k_{||} \neq 0$, which is a signature of discretization. The white curves are the fitting results of the maxima of the polariton dispersions (for the detailed procedure see Supplement 1).

The energy discretization of polariton branches can be explained by a theoretical model of trapped polaritons developed by Savona and coworkers [10] what we briefly summarize here for convenience. In their work, Maxwell equations are solved in cylindrical coordinates, assuming a circular "mesa" with a certain diameter. A discontinuous energy spectrum appears, reflecting discretized modes of the cavity photon. Then, they introduce the Schrödinger equation in which the exciton center-of-mass wave function is expressed in terms of the modes of a free particle; the coupling between exciton and photon modes is expressed in terms of the Rabi splitting of the planar cavity. Solving the Schrödinger equation then yields step-like discretized polariton energy levels. Similar results can also be found for etched micropillar cavities, where the parabolic cavity resonance splits into a set of discrete photonic modes due to the spatially confined circular waveguide geometry [43–45]. In that case, the discretization of the photonic modes is transferred to the polariton modes through exciton–photon coupling. Likewise, in our sample, we can attribute the observed discretized modes (Fig. 2(c)) to the action of the lateral confinement of the TMD polaritons, which is evidenced by the appearance of the "hot spots" in Fig. 2(b).

Despite the clear signatures of polariton trapping given by the spatial map of the PL intensity (Fig. 2(b)) and the induced dispersion discretization of each individual polariton mode observed in the energy-momentum-resolved PL map (Fig. 2(c)), direct evidence of coupling between the discretized polariton modes is missing. Thus, we carried out 2D micro-spectroscopy and obtained data with spatial resolution exclusively from one of the trapping areas (as indicated by the white arrow in Fig. 2(b)). We acquired spatially resolved 2D spectra at various waiting times T. Exemplarily, the rephasing and non-rephasing spectra at $T = 50$ fs are shown in Figs. 3(a) and 3(e), respectively. Both types of signals oscillate as the coherence times τ and t are scanned. In rephasing pathways, the signs of the oscillation frequencies are opposite to each other for the coherent state ($|e\rangle\langle g|$) created by the third pulse compared to the coherent state ($|g\rangle\langle e|$) created by the first pulse. By contrast, in non-rephasing pathways the coherent states created by the first and the third pulses have the same frequency sign. The sum of the two types of signals will result in "absorptive" spectra which can be related to the transient absorption spectra measured from pump–probe experiments by integrating the 2D spectra along the ω_τ axis. When quantum beating signals are of interest, separate analysis of the rephasing and non-rephasing 2D spectra becomes necessary, as done here, because the oscillating pathways that contribute to the beating signals are different in the two types of spectra, as discussed in Supplement 1.

By fitting the peak positions of diagonal peaks in the measured 2D spectra, we could reveal the energy structure of the single-excitation manifold [41]. In both types of spectra, three diagonal components are identified, corresponding to three polariton branches, as marked by the orange, purple, and green colored boxes in Fig. 3. We note that the lowest polariton branch (located at ~1.605 eV) found in the energy-momentum-resolved PL map was not detected by the 2D spectra because of the very low laser intensity at 1.605 eV, whereas an additional high-energy polariton branch located at ~1.678 eV not visible in the linear PL data could be revealed by the 2D measurements.

In addition to the above-mentioned three polariton branches (i.e., the diagonal components located at 1.633, 1.653, and 1.678 eV), we have further identified two higher-energy polariton branches (located at 1.702 and 1.730 eV) by moving the center of the laser spectrum to higher energy in previous work [41]. Therefore, 2D micro-spectroscopy, as opposed to linear PL spectroscopy, allowed us to obtain a more complete polariton energy structure. On the other hand, the trap-induced discretization of each branch (several meV splittings in energy as shown in Fig. 2(c)) could not be resolved in the 2D spectra because our measurements had an energy resolution (~20 meV) larger than the energy splittings between discretized polariton modes.

Optical Materials EXPRESS

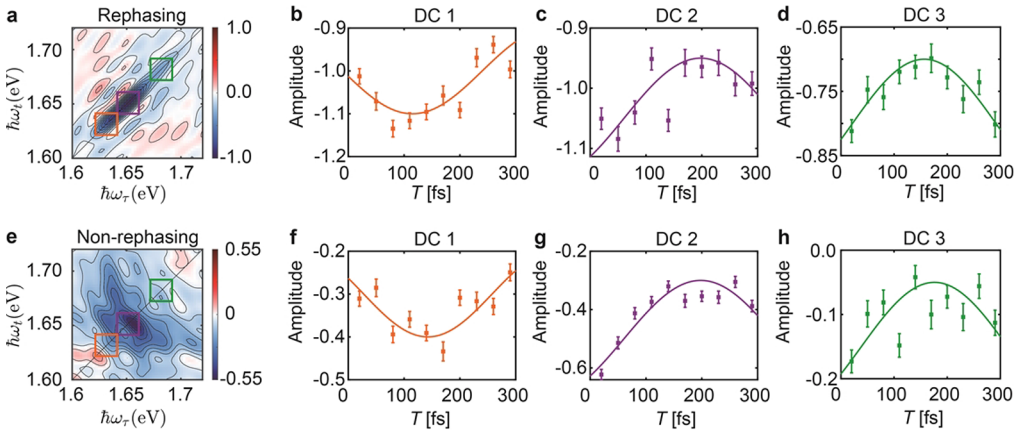

Fig. 3. Coherent 2D micro-spectroscopy results. Rephasing (a) and non-rephasing (e) 2D spectra at $T = 50$ fs. Amplitude evolutions (squares) and their fitting results (solid curves) of the rephasing (b–d) and the non-rephasing (f–h) spectra as a function of population time T for the diagonal components located at 1.633 eV (b and f, marked by orange regions of interest in a and e, respectively), 1.653 eV (c and g, marked by purple color), and 1.678 eV (d and h, marked by green color).

In addition, the focusing in the microscope objective led to an averaging over the transverse momentum coordinate from Fig. 2(c) because of the superposition of incident wave vectors in the focus. Despite the low energy resolution, we were able to utilize the time dependence of the 2D spectra as a function of population time, i.e., as a function of the time delay between the second and the third pulse of the incident four-pulse sequence, to detect quantum beats resulting from a superposition of polariton states. These results do not only reflect the existence of energy discretization, but also allow us to analyze the coupling between discretized polariton modes that is not visible in the conventional PL spectra, as we will discuss now.

In Fig. 3, we show the integrated amplitude for each diagonal polariton-branch component of the rephasing (Fig. 3(b)–(d)) and the non-rephasing (Fig. 3(f)–(h)) 2D spectra as a function of the waiting time T. Oscillating signals can be observed in all cases. The oscillations were fitted by cosine functions, with the fitting results shown as the solid curves in each panel of Figs. 3(b)–(d) and 3(f)–h. Fitting parameters are listed in Table 1. The oscillation time periods determined independently for all the curves have a mean value of 525 fs (corresponding to an energy of ~7.9 meV), with a statistical standard deviation of ~34 fs. This energy value agrees well with the energy splittings (~8 meV) determined by calculating the mean value of the energy differences between the neighboring platforms indicated by the white lines in the energy-momentum-resolved PL map (Fig. 2(c)), suggesting that the oscillations are likely to result from the interactions between these laterally confined discrete polariton states. On the other hand, the energy separations between the first and second parabolic polariton branches is ~0.0250 eV and between the second and third parabolic polariton branches ~0.0130 eV. These differences do not agree with the energy determined from the oscillating signals and thus cannot be the cause of the observed effect. Within the chosen detection window of the population time, it was not possible to extract the decoherence times of the observed beating signals. The phase of each oscillating curve, however, could be determined from the fits of the curves. The mean value of the phase of the rephasing and the non-rephasing signals shifts from -0.54π for the diagonal component at 1.633 eV to +0.28π for the diagonal component at 1.653 eV and to +0.39π for the diagonal component at 1.678 eV. Note that the reference point of the cosine oscillation phase is the value at $T = 0$.

Optical Materials EXPRESS

Table 1. Fitting parameters of the oscillations of the three diagonal polariton-branch components of the recorded 2D spectra. The reference point of the cosine oscillation phase is the value at $T = 0$.

Parameters[a]		1.633 eV	1.653 eV	1.678 eV
Rephasing signal	τ_p	500 fs	550 fs	540 fs
	φ	-0.46 π	0.28 π	0.42 π
Non-rephasing signal	τ_p	460 fs	550 fs	550 fs
	φ	-0.62 π	0.28 π	0.36 π
Mean value	τ_p	480 fs	550 fs	545 fs
	φ	-0.54 π	0.28 π	0.39 π

[a]Fit formula: $y = a\cos\left(\frac{2\pi T}{\tau_p} + \varphi\right) + b$, where y is the observed signal, a an amplitude, T the population time, τ_p the oscillation period, and φ the phase of the oscillation.

The quantum beats may be caused by two possible mechanisms. In the first case, by exciting the system with broadband laser pulses, a superposition between two electronically excited states can be created from which oscillating signals can be observed. However, as we confirm via 2D spectral simulation in Supplement 1, such a superposition of polariton modes gives rise to quantum beats with a phase of ~ 0 (or π) when fitting with a cosine function. This obviously does not agree with our experimental observation, where the phases vary with spectral position and are far away from 0 (or π).

The second possible mechanism of observing quantum beats is the creation of vibrational coherence. It has been found that the observed oscillatory phase of the quantum beats in ultrafast spectroscopy experiments can deviate from zero when electronic transitions are associated with the excitation of coherent phonons [46–49]. The theoretical mechanism behind such a beating phase modulation has been established by Garrett and coworkers [50]. The lattice motion induced by electronic transitions has two different modes: one arises from impulsive excitation and the other from displacive excitation, and there is a phase difference of π/2 between the beats resulting from the two modes. In the general case, the phase of oscillations may be found in between the two extremes, and thus can be arbitrary, just like we observe.

That is to say, the observed quantum beats show frequencies that agree with the difference frequencies between discretized polariton modes. Although, it is not possible to infer from the frequency alone whether phonons are involved in the coupling or not, the experimentally observed phase changes cannot be explained without the interaction with phonon. Based on the above reasons, we attribute the observed beating signals to the formation of phonons. To explain the mechanism, we adopt a vibronic coupling model [28,51]. In this model, the energy difference between the two discretized polariton modes is close to the overtone of an interlayer shearing mode between the TMD monolayer and hBN layers (Fig. 4). An electronic coupling between two polariton modes leads to a hybridization of the states $|e^1\rangle|1^{1e}\rangle$ (where polariton mode 1 is excited, $|e^1\rangle$, and the phonon mode is also excited, $|1^{1e}\rangle$) and $|e^2\rangle|0^{2e}\rangle$ (where polariton mode 2 is excited, $|e^2\rangle$, while the phonon mode is not excited, $|0^{2e}\rangle$). This results in new states $|2'\rangle = a|e^1\rangle|1^{1e}\rangle + b|e^2\rangle|0^{2e}\rangle$ and $|3'\rangle = c|e^1\rangle|1^{1e}\rangle + d|e^2\rangle|0^{2e}\rangle$, with $a^2 + c^2 = 1$ and $b^2 + d^2 = 1$. The coefficients are given by $a = -cos(\vartheta)$, $b = sin(\vartheta)$, $c = sin(\vartheta)$, $d = cos(\vartheta)$, with $\vartheta = \frac{1}{2}arctan\frac{J}{\Delta E}$, where J is the resonance coupling and ΔE is the difference between energies of the interacting states before hybridization. Even if the coupling J is small, mixing can still be substantial at resonance, i.e., when ΔE is close to 0. In this case, $\vartheta = 45°$, both states $|2'\rangle$ and $|3'\rangle$ are made up with equal contributions from the states $|e^1\rangle|1^{1e}\rangle$ and $|e^2\rangle|0^{2e}\rangle$ and thus inherit the vibrational character from $|e^1\rangle|1^{1e}\rangle$ and the large dipole moment from $|e^2\rangle|0^{2e}\rangle$. The

Optical Materials EXPRESS

states $|1'\rangle$ and $|4'\rangle$ are the same states as $|e^1\rangle|0^{1e}\rangle$ (where polariton mode 1 is excited, $|e^1\rangle$, and the phonon mode is not excited, $|0^{1e}\rangle$) and $|e^2\rangle|1^{2e}\rangle$ (where polariton mode 2 is excited, $|e^2\rangle$, and the phonon mode is also excited, $|1^{2e}\rangle$), respectively. Coherent states $|1'2'|$ and $|1'3'|$ can be generated after two interactions with the light field, leading to an electronic population state and to a coherence within that first-excited-state manifold. This gives rise to coherent phonon emission and the quantum beats observed in our experiments. The phase of the oscillating signal in the time-resolved experiment depends on whether an impulsive or a displacive excitation dominates the coherent phonon generation.

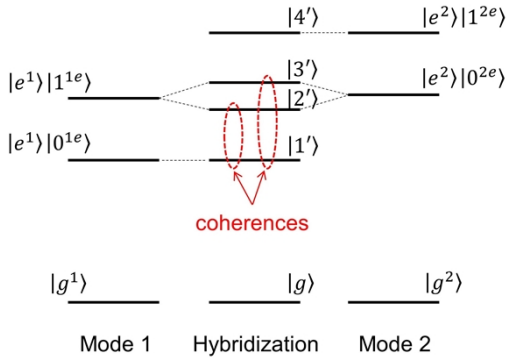

Fig. 4. Schematic illustration of vibronic coupling. The electronic coupling between two polariton modes results in the hybridization of the states $|e^1\rangle|1^{1e}\rangle$ and $|e^2\rangle|0^{2e}\rangle$, forming new states $|2'\rangle$ and $|3'\rangle$. Coherences (dashed red circles) between the states $|1'\rangle$ and $|2'\rangle$, and between $|1'\rangle$ and $|3'\rangle$, can be generated after double interaction with the light field, leading to the observed quantum beats.

4. Conclusion

We explored the coupling between discretized exciton-polariton modes in a micro-sized spatial trap inside a microcavity with an embedded van-der-Waals heterostructure at room temperature via photoluminescence-(PL-) detected, two-dimensional (2D) micro-spectroscopy. The confinement of the polariton was confirmed by a spatial map of the PL intensity, and the confinement-induced energy discretization was observed in an energy-momentum-resolved PL map. While these linear PL characterizations could not provide sufficient information to verify the coupling between discretized polariton modes, 2D micro-spectroscopy enabled us to detect quantum beats exclusively from a trap. Our results showed a wide phase variation of the 2D spectral amplitude oscillations, implying the existence of a coupling between the discretized polariton modes, which is accompanied by the generation of coherent phonon. The investigation of the coherent characteristics of the coupling between discretized polariton modes of microcavities can provide new insight for dynamical control of polariton relaxation and phonon generation through spatial confinement in future applications.

Funding. National Natural Science Foundation of China (22250002); Fundamental Research Funds for the Central Universities; European Research Council (679288); Japan Society for the Promotion of Science (19H05790, 20H00354, 21H05233); U.S. Department of Energy (SC0020653); Division of Electrical, Communications and Cyber Systems (2052527); Division of Materials Research (2111812); Division of Civil, Mechanical and Manufacturing Innovation (2129412); Bundesministerium für Bildung und Forschung (FKZ 13XP5053A); European Social Fund (2021FGI0043); Freistaat Thüringen (2021FGI0043); Julius-Maximilians-Universität Würzburg (Open Access Publication Fund).

Disclosures. The authors declare that there are no conflicts of interest related to this article.

Data availability. The data that support the findings of this study are available from the corresponding author upon reasonable request.

Optical Materials EXPRESS

Supplemental document. See Supplement 1 for supporting content.

References

1. C. Weisbuch, M. Nishioka, A. Ishikawa, and Y. Arakawa, "Observation of the coupled exciton-photon mode splitting in a semiconductor quantum microcavity," Phys. Rev. Lett. **69**(23), 3314–3317 (1992).
2. J. Kasprzak, M. Richard, S. Kundermann, A. Baas, P. Jeambrun, J. M. J. Keeling, F. M. Marchetti, M. H. Szymańska, R. André, J. L. Staehli, V. Savona, P. B. Littlewood, B. Deveaud, and L. S. Dang, "Bose–Einstein condensation of exciton polaritons," Nature **443**(7110), 409–414 (2006).
3. J. D. Plumhof, T. Stöferle, L. Mai, U. Scherf, and R. F. Mahrt, "Room-temperature Bose–Einstein condensation of cavity exciton–polaritons in a polymer," Nat. Mater. **13**(3), 247–252 (2014).
4. L. V. Butov, C. W. Lai, A. L. Ivanov, A. C. Gossard, and D. S. Chemla, "Towards Bose–Einstein condensation of excitons in potential traps," Nature **417**(6884), 47–52 (2002).
5. M. M. de Lima, M. van der Poel, P. V. Santos, and J. M. Hvam, "Phonon-induced polariton superlattices," Phys. Rev. Lett. **97**(4), 045501 (2006).
6. R. Balili, V. Hartwell, D. Snoke, L. Pfeiffer, and K. West, "Bose-Einstein condensation of microcavity polaritons in a trap," Science **316**(5827), 1007–1010 (2007).
7. E. A. Cerda-Méndez, D. Sarkar, D. N. Krizhanovskii, S. S. Gavrilov, K. Biermann, M. S. Skolnick, and P. V. Santos, "Exciton-polariton gap solitons in two-dimensional lattices," Phys. Rev. Lett. **111**(14), 146401 (2013).
8. D. Sarchi and V. Savona, "Long-range order in the Bose-Einstein condensation of polaritons," Phys. Rev. B **75**(11), 115326 (2007).
9. D. Bajoni, E. Peter, P. Senellart, J. L. Smirr, I. Sagnes, A. Lemaître, and J. Bloch, "Polariton parametric luminescence in a single micropillar," Appl. Phys. Lett. **90**(5), 051107 (2007).
10. R. I. Kaitouni, O. El Daïf, A. Baas, M. Richard, T. Paraiso, P. Lugan, T. Guillet, F. Morier-Genoud, J. D. Ganière, J. L. Staehli, V. Savona, and B. Deveaud, "Engineering the spatial confinement of exciton polaritons in semiconductors," Phys. Rev. B **74**(15), 155311 (2006).
11. C. Schneider, K. Winkler, M. D. Fraser, M. Kamp, Y. Yamamoto, E. A. Ostrovskaya, and S. Höfling, "Exciton-polariton trapping and potential landscape engineering," Rep. Prog. Phys. **80**(1), 016503 (2017).
12. T. K. Paraïso, D. Sarchi, G. Nardin, R. Cerna, Y. Leger, B. Pietka, M. Richard, O. El Daïf, F. Morier-Genoud, V. Savona, and B. Deveaud-Plédran, "Enhancement of microcavity polariton relaxation under confinement," Phys. Rev. B **79**(4), 045319 (2009).
13. G. Grosso, S. Trebaol, M. Wouters, F. Morier-Genoud, M. T. Portella-Oberli, and B. Deveaud, "Nonlinear relaxation and selective polychromatic lasing of confined polaritons," Phys. Rev. B **90**(4), 045307 (2014).
14. A. S. Kuznetsov, K. Biermann, and P. V. Santos, "Dynamic acousto-optical control of confined polariton condensates: From single traps to coupled lattices," Phys. Rev. Res. **1**(2), 023030 (2019).
15. X. Zhang, Y. Zhang, H. Dong, B. Tang, D. Li, C. Tian, C. Xu, and W. Zhou, "Room temperature exciton–polariton condensate in an optically-controlled trap," Nanoscale **11**(10), 4496–4502 (2019).
16. D. Ballarini, I. Chestnov, D. Caputo, M. De Giorgi, L. Dominici, K. West, L. N. Pfeiffer, G. Gigli, A. Kavokin, and D. Sanvitto, "Self-Trapping of Exciton-Polariton Condensates in GaAs Microcavities," Phys. Rev. Lett. **123**(4), 047401 (2019).
17. M. Wurdack, E. Estrecho, S. Todd, T. Yun, M. Pieczarka, S. K. Earl, J. A. Davis, C. Schneider, A. G. Truscott, and E. A. Ostrovskaya, "Motional narrowing, ballistic transport, and trapping of room-temperature exciton polaritons in an atomically-thin semiconductor," Nat. Commun. **12**(1), 5366 (2021).
18. D. L. Chafatinos, A. S. Kuznetsov, S. Anguiano, A. E. Bruchhausen, A. A. Reynoso, K. Biermann, P. V. Santos, and A. Fainstein, "Polariton-driven phonon laser," Nat. Commun. **11**(1), 4552 (2020).
19. X. Liu, T. Galfsky, Z. Sun, F. Xia, E. Lin, Y.-H. Lee, S. Kéna-Cohen, and V. M. Menon, "Strong light–matter coupling in two-dimensional atomic crystals," Nat. Photonics **9**(1), 30–34 (2015).
20. N. Lundt, S. Klembt, E. Cherotchenko, S. Betzold, O. Iff, A. V. Nalitov, M. Klaas, C. P. Dietrich, A. V. Kavokin, S. Höfling, and C. Schneider, "Room-temperature Tamm-plasmon exciton-polaritons with a WSe_2 monolayer," Nat. Commun. **7**(1), 13328 (2016).
21. S. Dufferwiel, S. Schwarz, F. Withers, A. a, P. Trichet, F. Li, M. Sich, O. D. Pozo-Zamudio, C. Clark, A. Nalitov, D. D. Solnyshkov, G. Malpuech, K. S. Novoselov, J. M. Smith, M. S. Skolnick, D. N. Krizhanovskii, and A. I. Tartakovskii, "Exciton–polaritons in van der Waals heterostructures embedded in tunable microcavities," Nat. Commun. **6**(1), 8579 (2015).
22. H. Shan, L. Lackner, B. Han, E. Sedov, C. Rupprecht, H. Knopf, F. Eilenberger, J. Beierlein, N. Kunte, M. Esmann, K. Yumigeta, K. Watanabe, T. Taniguchi, S. Klembt, S. Höfling, A. V. Kavokin, S. Tongay, C. Schneider, and C. Antón-Solanas, "Spatial coherence of room-temperature monolayer WSe_2 exciton-polaritons in a trap," Nat. Commun. **12**(1), 6406 (2021).
23. T. Brixner, J. Stenger, H. M. Vaswani, M. Cho, R. E. Blankenship, and G. R. Fleming, "Two-dimensional spectroscopy of electronic couplings in photosynthesis," Nature **434**(7033), 625–628 (2005).
24. S. Mukamel, "Multidimensional femtosecond correlation spectroscopies of electronic and vibrational excitations," Annu. Rev. Phys. Chem. **51**(1), 691–729 (2000).
25. M. Cho, "Coherent two-dimensional optical spectroscopy," Chem. Rev. **108**(4), 1331–1418 (2008).

Optical Materials EXPRESS

26. N. S. Ginsberg, Y.-C. Cheng, and G. R. Fleming, "Two-dimensional electronic spectroscopy of molecular aggregates," Acc. Chem. Res. **42**(9), 1352–1363 (2009).
27. G. Moody and S. T. Cundiff, "Advances in multi-dimensional coherent spectroscopy of semiconductor nanostructures," Advances in Physics: X **2**(3), 641–674 (2017).
28. N. Christensson, H. F. Kauffmann, T. Pullerits, and T. Mančal, "Origin of long-lived coherences in light-harvesting complexes," J. Phys. Chem. B **116**(25), 7449–7454 (2012).
29. E. Harel and G. S. Engel, "Quantum coherence spectroscopy reveals complex dynamics in bacterial light-harvesting complex 2 (LH2)," Proc. Natl. Acad. Sci. U. S. A. **109**(3), 706–711 (2012).
30. R. Tempelaar, T. L. C. Jansen, and J. Knoester, "Vibrational beatings conceal evidence of electronic coherence in the FMO light-harvesting complex," J. Phys. Chem. B **118**(45), 12865–12872 (2014).
31. E. Thyrhaug, R. Tempelaar, M. J. P. Alcocer, K. Žídek, D. Bína, J. Knoester, T. L. C. Jansen, and D. Zigmantas, "Identification and characterization of diverse coherences in the Fenna–Matthews–Olson complex," Nat. Chem. **10**(7), 780–786 (2018).
32. Y. Song, S. N. Clafton, R. D. Pensack, T. W. Kee, and G. D. Scholes, "Vibrational coherence probes the mechanism of ultrafast electron transfer in polymer–fullerene blends," Nat. Commun. **5**(1), 4933 (2014).
33. A. De Sio, F. Troiani, M. Maiuri, J. Réhault, E. Sommer, J. Lim, S. F. Huelga, M. B. Plenio, C. A. Rozzi, G. Cerullo, E. Molinari, and C. Lienau, "Tracking the coherent generation of polaron pairs in conjugated polymers," Nat. Commun. **7**(1), 13742 (2016).
34. L. Wang, G. B. Griffin, A. Zhang, F. Zhai, N. E. Williams, R. F. Jordan, and G. S. Engel, "Controlling quantum-beating signals in 2D electronic spectra by packing synthetic heterodimers on single-walled carbon nanotubes," Nat. Chem. **9**(3), 219–225 (2017).
35. S. Sim, D. Lee, A. V. Trifonov, T. Kim, S. Cha, J. H. Sung, S. Cho, W. Shim, M.-H. Jo, and H. Choi, "Ultrafast quantum beats of anisotropic excitons in atomically thin ReS_2," Nat. Commun. **9**(1), 351 (2018).
36. D. Li, C. Trovatello, S. Dal Conte, M. Nuß, G. Soavi, G. Wang, A. C. Ferrari, G. Cerullo, and T. Brixner, "Exciton–phonon coupling strength in single-layer $MoSe_2$ at room temperature," Nat. Commun. **12**(1), 954 (2021).
37. S. Goetz, D. Li, V. Kolb, J. Pflaum, and T. Brixner, "Coherent two-dimensional fluorescence micro-spectroscopy," Opt. Express **26**(4), 3915–3925 (2018).
38. V. Tiwari, Y. A. Matutes, A. T. Gardiner, T. L. C. Jansen, R. J. Cogdell, and J. P. Ogilvie, "Spatially-resolved fluorescence-detected two-dimensional electronic spectroscopy probes varying excitonic structure in photosynthetic bacteria," Nat. Commun. **9**(1), 4219 (2018).
39. D. Li, E. Titov, M. Roedel, V. Kolb, S. Goetz, R. Mitric, J. Pflaum, and T. Brixner, "Correlating nanoscale optical coherence length and microscale topography in organic materials by coherent two-dimensional micro-spectroscopy," Nano Lett. **20**(9), 6452–6458 (2020).
40. H. Knopf, N. Lundt, T. Bucher, S. Höfling, S. Tongay, T. Taniguchi, K. Watanabe, I. Staude, U. Schulz, C. Schneider, and F. Eilenberger, "Integration of atomically thin layers of transition metal dichalcogenides into high-Q, monolithic Bragg-cavities: An experimental platform for the enhancement of the optical interaction in 2D-materials," Opt. Mater. Express **9**(2), 598–610 (2019).
41. D. Li, H. Shan, C. Rupprecht, H. Knopf, K. Watanabe, T. Taniguchi, Y. Qin, S. Tongay, M. Nuß, S. Schröder, F. Eilenberger, S. Höfling, C. Schneider, and T. Brixner, "Hybridized exciton-photon-phonon states in a transition metal Dichalcogenide van der Waals heterostructure microcavity," Phys. Rev. Lett. **128**(8), 087401 (2022).
42. S. Latini, U. De Giovannini, E. J. Sie, N. Gedik, H. Hübener, and A. Rubio, "Phonoritons as hybridized exciton-photon-phonon excitations in a monolayer h-BN optical cavity," Phys. Rev. Lett. **126**(22), 227401 (2021).
43. A. G. Silva, C. A. Parra-Murillo, P. T. Valentim, J. S. V. Morais, F. Plentz, P. S. S. Guimarães, H. Vinck-Posada, B. A. Rodriguez, M. S. Skolnick, A. Tahraoui, and M. Hopkinson, "Quantum dot dipole orientation and excitation efficiency of micropillar modes," Opt. Express **16**(23), 19201–19207 (2008).
44. S. M. Ulrich, C. Gies, S. Ates, J. Wiersig, S. Reitzenstein, C. Hofmann, A. Löffler, A. Forchel, F. Jahnke, and P. Michler, "Photon statistics of semiconductor microcavity lasers," Phys. Rev. Lett. **98**(4), 043906 (2007).
45. S. Reitzenstein and A. Forchel, "A. Quantum dot micropillars," J. Phys. D: Appl. Phys. **43**(3), 033001 (2010).
46. G. C. Cho, W. Kütt, and H. Kurz, "Subpicosecond time-resolved coherent-phonon oscillations in GaAs," Phys. Rev. Lett. **65**(6), 764–766 (1990).
47. T. Pfeifer, W. Kütt, H. Kurz, and R. Scholz, "Generation and detection of coherent optical phonons in germanium," Phys. Rev. Lett. **69**(22), 3248–3251 (1992).
48. A. Yamamoto, T. Mishina, Y. Masumoto, and M. Nakayama, "Coherent oscillation of zone-folded phonon modes in GaAs-AlAs superlattices," Phys. Rev. Lett. **73**(5), 740–743 (1994).
49. Y. Liu, A. Frenkel, G. A. Garrett, J. F. Whitaker, S. Fahy, C. Uher, and R. Merlin, "Impulsive light scattering by coherent phonons in $LaAlO_3$: Disorder and boundary effects," Phys. Rev. Lett. **75**(2), 334–337 (1995).
50. G. A. Garrett, T. F. Albrecht, J. F. Whitaker, and R. Merlin, "Coherent THz phonons driven by light pulses and the Sb problem: What is the mechanism?" Phys. Rev. Lett. **77**(17), 3661–3664 (1996).
51. S. Polyutov, O. Kühn, and T. Pullerits, "Exciton-vibrational coupling in molecular aggregates: Electronic versus vibronic dimer," Chem. Phys. **394**(1), 21–28 (2012).